Nonlinearity and Finite-Time Instability in a T21L3 Quasigeostrophic Model*

JIANG Zhina†(姜智娜) and WANG Donghai(王东海)

State Key Laboratory of Severe Weather, Chinese Academy of Meteorological Sciences, Beijing 100081

(Received May 18, 2010; in final form March 24, 2011)

ABSTRACT

In this paper, a nonlinear optimization method is used to explore the finite-time instability of the atmospheric circulation with a three-level quasigeostrophic model under the framework of the conditional nonlinear optimal perturbation (CNOP). As a natural generalization of linear singular vector (SV), CNOP is defined as an initial perturbation that makes the cost function the maximum at a prescribed forecast time under certain physical constraint conditions. Special attentions are paid to the different structures and energy evolutions of the optimal perturbations.

The results show that the most instable region of the global atmospheric circulation lies in the midlatitude Eurasian continent. More specially, SV and CNOP in the total energy norm with an optimization time of 2 days both present localness: they are mainly located in the midlatitude Asian continent and its east coast. With extension of the optimization time, SVs are more upstream and less localized in the zonal direction, and CNOPs differ essentially from SVs with broader zonal and meridional coverages; as a result, CNOPs acquire larger kinetic and available potential energy amplifications than SVs in the nonlinear model at the corresponding optimization time. For the climatological wintertime flow, it is seen that the baroclinic terms remain small over the entire time evolution, and the energy production comes essentially from the eddy kinetic energy, which is induced by the horizontal shear of the basic flow.

In addition, the effects of SVs and CNOPs on the Eurasian atmospheric circulation are explored. The results show that the weather systems over the Eurasian continent in the perturbed fields by CNOPs are stronger than those by SVs at the optimization time. This reveals that the CNOP method is better in evaluating the instability of the atmospheric circulation while the SV method underestimates the possibility of extreme weather events.

Key words: nonlinearity, finite-time instability, barotropic, baroclinic

Citation: Jiang Zhina and Wang Donghai, 2011: Nonlinearity and finite-time instability in a T21L3 quasigeostrophic model. *Acta Meteor. Sinica*, **25**(4), 419–429, doi: 10.1007/s13351-011-0403-2.

1. Introduction

The atmosphere is a complicated nonlinear chaotic system (Lorenz, 1963). Small perturbations in initial conditions may greatly influence the numerical weather forecasting, e.g., the weather regime transition is very sensitive to small initial perturbations (Molteni and Palmer, 1993; Oortwijn and Barkmeijer, 1995; Li et al., 1999; Frederiksen, 2000). The method of singular vectors (SVs) is popularly used in the studies of atmospheric instability and predictability, which was first proposed in the meteorological context by Lorenz (1965). An SV is defined in such a way as to maximize the growth rate in a specified norm over a given time interval. Note that SVs are computed in a linear context. However, the linear approximation is not valid for synoptic systems beyond two days.

Mu et al. (2003) proposed a new method called conditional nonlinear optimal perturbation (CNOP), which is an extension of the SV method into the nonlinear regime. CNOP is actually an initial perturbation that makes the cost function the maximum at a prescribed forecast time under certain physical constraint conditions. Since the publication of this new

*Supported by the National Natural Science Foundation of China (40905023) and Basic Research Program of State Key Laboratory of Severe Weather, Chinese Academy of Meteorological Sciences (2008LASWZI01).

†Corresponding author: jzn@cams.cma.gov.cn.

method, a number of studies have been conducted to compare it with the SV method. Mu and Zhang (2006) explored the characteristics of CNOPs in energy norm, and revealed that when the linear approximation is valid, CNOP resembles SV; however, when the linear approximation is invalid, there exist considerable differences between CNOP and SV in the energy structure and growth rate. By using a T21L3 quasigeostrophic (QG) model, Jiang et al. (2008) revealed that CNOPs do depend, as SVs do, on the norm chosen. The streamfunction squared norm yields small-scale disturbances while the results obtained by the total energy norm are characterized by intermediate-scale disturbances, and in case of the enstrophy norm, CNOPs are typified by large-scale disturbances with a large zonal flow contribution. Riviere et al. (2008) pointed out that CNOPs in the total energy norm differ from SVs in the presence of a positive zonal-mean shear at initial time and in a broader meridional extension in a baroclinic unstable flow which is assumed zonally symmetric but with opposite zonal velocities in the upper and lower layers. Furthermore, the physical mechanisms of optimal perturbation growth are explained. Motivated by the above work, we now apply the CNOP method to more realistic situations, e.g., a climatological wintertime flow, by using a T21L3 QG model, which is capable of describing blocking and strong zonal flow regimes in a realistic way. We aim to explore the finite-time instability of global circulation by use of CNOP in comparison with SV. Moreover, the physical mechanisms of the growth of optimal perturbations and their effects on the atmospheric circulations can be further investigated. These allow us to better understand the role of nonlinearities in the atmospheric instability.

The paper is arranged as follows. In Section 2, the T21 QG model and the nonlinear optimization method are introduced. In Section 3, we compare the properties of SVs and CNOPs, especially their spatial patterns. Section 4 explores the energy evolutions of SVs and CNOPs. In addition, the effect of optimal perturbations on the Eurasian atmospheric circulation is examined in Section 5. The conclusions are summarized in Section 6.

2. Model description and the CNOP method

2.1 Model

The quasigeostrophic model used in this study is a global spectral model with the triangular truncation T21 and three levels in the vertical (Marshall and Molteni, 1993). The QG potential vorticity (PV) is the prognostic variable. The governing equations are

$$\frac{\partial q_1}{\partial t} = -J(\psi_1, q_1) - D_1(\psi_1, \psi_2) + S_1,$$
$$\frac{\partial q_2}{\partial t} = -J(\psi_2, q_2) - D_2(\psi_1, \psi_2, \psi_3) + S_2,$$
$$\frac{\partial q_3}{\partial t} = -J(\psi_3, q_3) - D_3(\psi_2, \psi_3) + S_3,$$

where the index $i = 1$, 2, and 3 refers to 200, 500, and 800 hPa, respectively. Here, PV is defined as

$$q_1 = \nabla^2\psi_1 - R_1^{-2}(\psi_1 - \psi_2) + f,$$
$$q_2 = \partial^2\psi_2 + R_1^{-2}(\psi_1 - \psi_2) - R_2^{-2}(\psi_2 - \psi_3),$$
$$q_3 = \nabla^2\psi_3 + R_2^{-2}(\psi_2 - \psi_3) + f(1 + \frac{h}{H_0}),$$

where $f = 2\Omega\sin\phi$, and $R_1 = 700$ km and $R_2 = 450$ km are Rossby radii of deformation appropriate to the 200–500-hPa layer and the 500–800-hPa layer, respectively. The variable h is the real orographic height, and H_0 is a scale height (9 km). $J(\psi, q)$ is the Jacobian operator. D_1, D_2, and D_3 are linear operators representing respectively the effects of Newtonian relaxation of temperature, linear drag on the 800-hPa wind, and horizontal diffusion of vorticity and temperature. S_1, S_2, and S_3 are time independent but spatially varying sources of PV that are necessary to obtain a realistic climatology from nonlinear integrations of the model. The exact form adopted for these operators can be found in the paper by Marshall and Molteni (1993).

2.2 The CNOP method

With $\boldsymbol{Q}$ denoting the column vector of PV spectral coefficients, we can formally write the spectral equations in the form

$$\frac{\mathrm{d}\boldsymbol{Q}}{\mathrm{d}t} = N[\boldsymbol{Q}(t)], \tag{1}$$

where N denotes a nonlinear matrix operator.

Assume that for fixed $T > 0$ and the initial potential vorticity $\boldsymbol{Q}_0$, the propagator M is well–defined; then $\boldsymbol{Q}(T) = M_T(\boldsymbol{Q}_0)$ is the solution of Eq. (1) at time T.

In the following numerical experiments, the total energy norm is adopted to constraint the amplitude of initial perturbations and to measure the magnitude of perturbation growth, which is defined as,

$$\| q \|_E^2 = -\int q\varphi \mathrm{d}V,$$

where the variables are all integrated over the whole atmosphere V. The variable q is the potential vorticity perturbation. The streamfunction perturbation is defined as $\varphi = \boldsymbol{E}^{-1}q$, where $\boldsymbol{E}$ is the linear operator that transforms streamfunction into potential vorticity and $\boldsymbol{E}^{-1}$ is the inverse operator, which transforms potential vorticity into streamfunction.

CNOP is defined as an initial perturbation that makes the objective function obtain the maximum value under the initial constraint condition $\|q_0\|_E \leqslant \sigma$. That is,

$$J(q_0^*) = \max_{\|q_0\|_E \leqslant \sigma} J(q_0),$$

where

$$J(q_0) = \| M_T(Q_0 + q_0) - M_T(Q_0) \|_E,$$

and q_0 is a given initial potential vorticity perturbation, which satisfies $\|q_0\|_E \leqslant \sigma$. The variable σ is a presumed positive constant representing an upper bound of the magnitude of the initial perturbation.

Solving the above maximum problem is equivalent to tackling the following minimum problem,

$$J_1(q_0^*) = \min_{\|q_0\|_E \leqslant \sigma} J_1(q_0),$$

where

$$J_1(q_0) = -(J(q_0))^2 = -\| M_T(Q_0 + q_0) - M_T(Q_0) \|_E^2 .$$

The first variation of $J_1(q_0)$ is

$$\begin{aligned}\delta J_1(q_0) = -\big\{&2\boldsymbol{M}^{*E}(Q_0 + q_0)[M_T(Q_0 + q_0) \\ &-M_T(Q_0)], \delta q_0\big\}_E\end{aligned}$$

In the numerical model used in this study, the adjoint $\boldsymbol{M}^*$ of the tangent version of the model equations has been defined with respect to the entrophy inner product. According to Buizza et al. (1993), the adjoint operator $\boldsymbol{M}^{*E}$ with respect to the above total energy norm can be deduced from $\boldsymbol{M}^*$. Hence, $\boldsymbol{M}^{*E} = \boldsymbol{E}\boldsymbol{M}^*\boldsymbol{E}^{-1}$. Then

$$\begin{aligned}\delta J_1(q_0) &= -\big\{2\boldsymbol{E}\boldsymbol{M}^*(Q_0 + q_0))\boldsymbol{E}^{-1} \\ &\quad \cdot\big[M_T(Q_0 + q_0) - M_T(Q_0)\big], \delta q_0\big\}_E \\ &= (\nabla J_1, \delta q_0)_E,\end{aligned}$$

where ∇J_1 is the gradient of the new objective function J_1 with respect to initial perturbation q_0. The optimization algorithm of the spectral projected gradient 2 (SPG2) can be used to calculate the least value (a local or global minimum) of a function of several variables subject to box or ball constraints (Birgin et al., 2000), which needs the objective function and its gradient of initial perturbations. The above deductions have provided the conditions to use the SPG2 method, and then the nonlinear optimization problem can be solved numerically.

To compare with the CNOP method, the first SV is also generated using the SPG2 method with the smallest constraint condition. Here, the objective function for SV is a modified version of CNOP, which is obtained by replacing the nonlinear evolution of the initial perturbation by integrating the tangent linear model.

Besides, to quantify the degree of similarity between SV and CNOP, the similarity index S, according to Buizza (1994) and Kim et al. (2004), is defined as

$$S = \langle e_1, e_2 \rangle / \| e_1 \|_{L_2} / \| e_2 \|_{L_2},$$

where e_1 and e_2 represent the streamfunction fields of SV and CNOP, respectively.

$$\| e_i \|_{L_2}^2 = \langle e_i, e_i \rangle = \int (e_i \cdot e_i)\mathrm{d}V, \quad (i = 1, 2).$$

The larger the value S is, the more similar the two patterns are.

3. SVs and CNOPs in a climatological flow

In this section, the first SVs and CNOPs are calculated in a climatological flow at the optimization time of 2, 5, and 8 days, respectively. The initial constraint condition $\sigma = 1.0$ (m s^{-1}) is adopted so that the initial maximum amplitude is within 20 gpm at 500 hPa. Figure 1 shows the 500-hPa streamfunction and zonal wind of the climatological flow, which is constructed from a 1800-day integration of the T21L3 QG model with the European Center for Medium-range Weather Forecasting (ECMWF) analysis of 0000 UTC 1 December 1983 as the initial condition. The simulated climatological flow is identical to the observed one with three low troughs and three high ridges.

Figure 2 shows the first SVs, optimized for days 2, 5, and 8, together with their evolutions at 500 hPa at their respective optimization time in the nonlinear model. For the initial SVs, they are all concentrated in the Northern Hemisphere, with a maximum value appearing close to the midlatitude and small values in the tropics. For the 2-day SV (Fig. 2a), it is found that the structure is highly localized over the Asian continent and its east coast. From Figs. 2b and 2c, we find that the 5- and 8-day SVs are more upstream, covering the whole Eurasian continent. During the time evolution, the SVs increase their spatial coverages and propagate eastward to the Pacific area (Figs. 2d, 2e, and 2f).

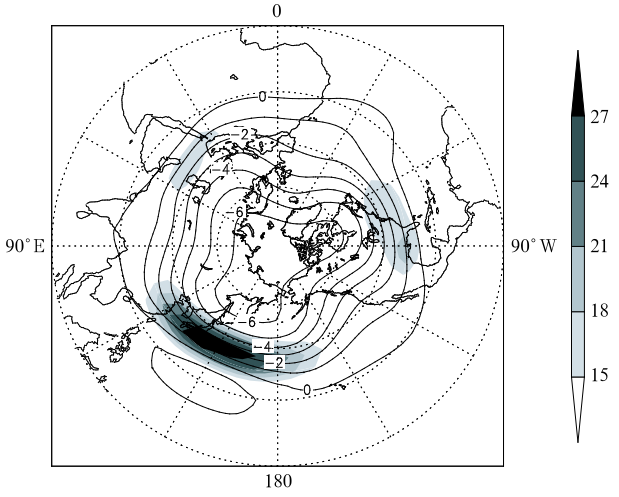

Fig. 1. The 500-hPa streamfunction ($\times 10^7$m^2 s^{-1}; contour) and zonal wind (m s^{-1}; shaded) of the climatological flow constructed from a 1800-day integration by using the T21L3 QG model with ECMWF analysis of 0000 UTC 1 December 1983 as the initial condition.

Similarly, the CNOPs, optimized for days 2, 5, and 8, together with their nonlinear evolutions at 500 hPa at their respective optimization time are shown in Fig. 3. For the optimization time of 2 days (Fig. 3a), the initial CNOP resembles the corresponding SV. However, with extension of the optimization time, the initial CNOPs show great differences to the corresponding SVs. The CNOPs, optimized for 5 and 8 days (Figs. 3b and 3c), are less localized in both the zonal and meridional directions. The 8-day CNOP is even distributed in the whole zonal direction. Similar to SVs, CNOPs increase their spatial scales and propagate eastward to the Pacific area (Figs. 3d, 3e, and 3f) as time goes by.

The similarity index between SV and CNOP for different optimization times is listed in Table 1. For the optimization time of 2 days, the similarity index is very large. That is to say, the linear approximation is valid. The similarity index decreases with the optimization time, which means that the nonlinearity plays an increasingly important role and CNOP can then better capture the characteristics of the nonlinearity.

Table 1. The similarity index between SV and CNOP for different optimization times

	Climatological flow	
	SV	CNOP
2 days	96.5%	
5 days	45.0%	
8 days	7.9%	

4. The optimal perturbation evolution

In order to see the energy source for the optimal perturbations, we first decompose the potential vorticity q_i into a perturbation q_i' and a basic state $\overline{q_i}$; similarly, streamfunction $\psi_i = \psi_i' + \overline{\psi_i}$. The PV perturbation equation is written as

$$\frac{\partial q_i'}{\partial t} = -J(\overline{\psi_i}, q_i') - J(\psi_i', \overline{q_i}) - J(\psi_i', q_i') - D_i, \qquad (2)$$

where $i = 1, 2, 3$. PV perturbation is given as follows:

$$q_1' = \nabla^2 \psi_1' - R_1^{-2}(\psi_1' - \psi_2'),$$

$$q_2' = \nabla^2\psi_2' + R_1^{-2}(\psi_1' - \psi_2') - R_2^{-2}(\psi_2' - \psi_3'),$$
$$q_3' = \nabla^2\psi_3' + R_2^{-2}(\psi_2' - \psi_3').$$

Then, multiplying Eq. (2) by $-\psi_i'$, horizontally averaging the equation, and summing over the

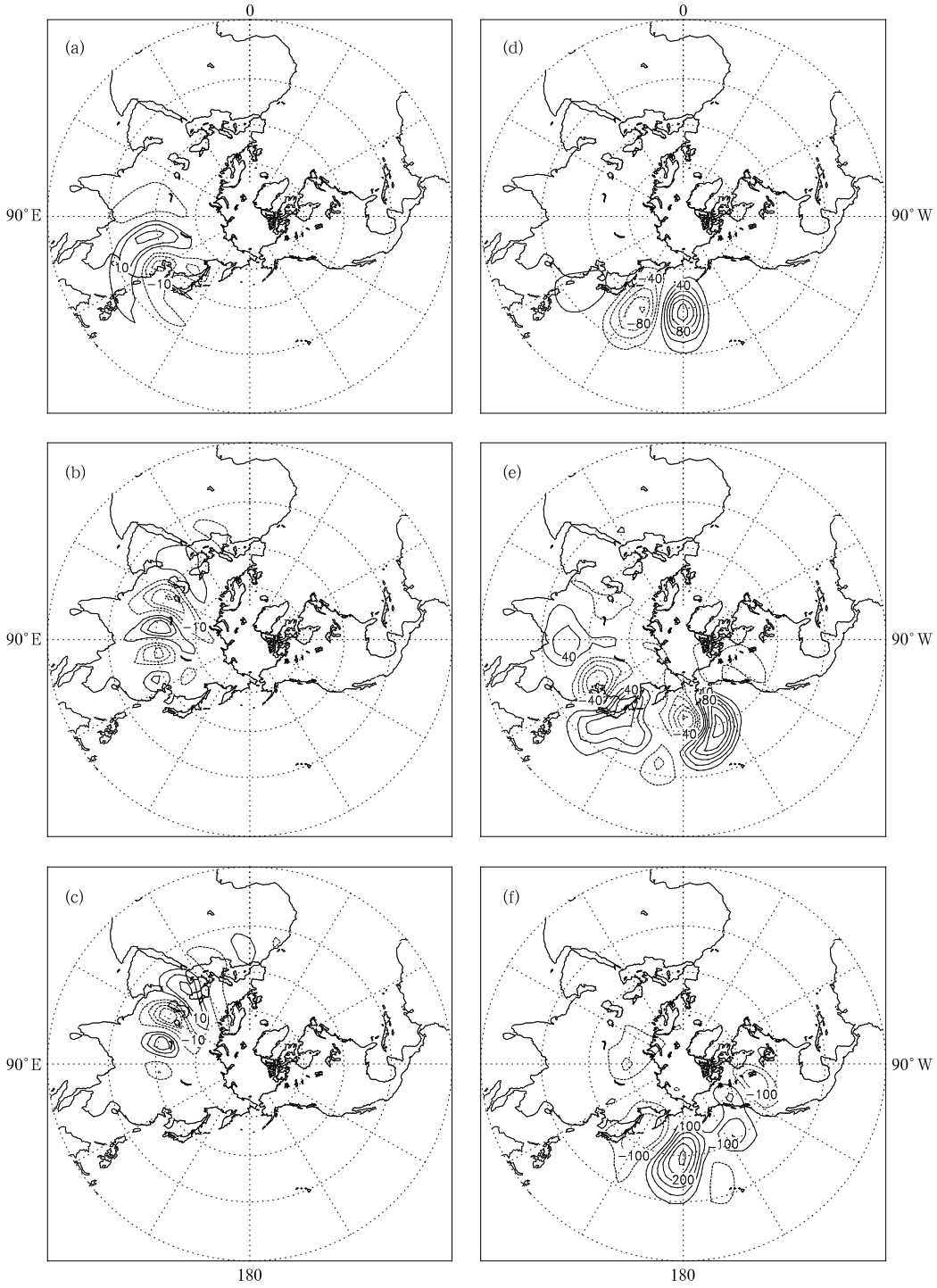

Fig. 2. 500-hPa geopotential height (gpm) of the first SVs, optimized for days 2 (a), 5 (b) and 8 (c), together with their evolutions at the optimization time of 2 (d), 5 (e), and 8 (f) days in the nonlinear model.

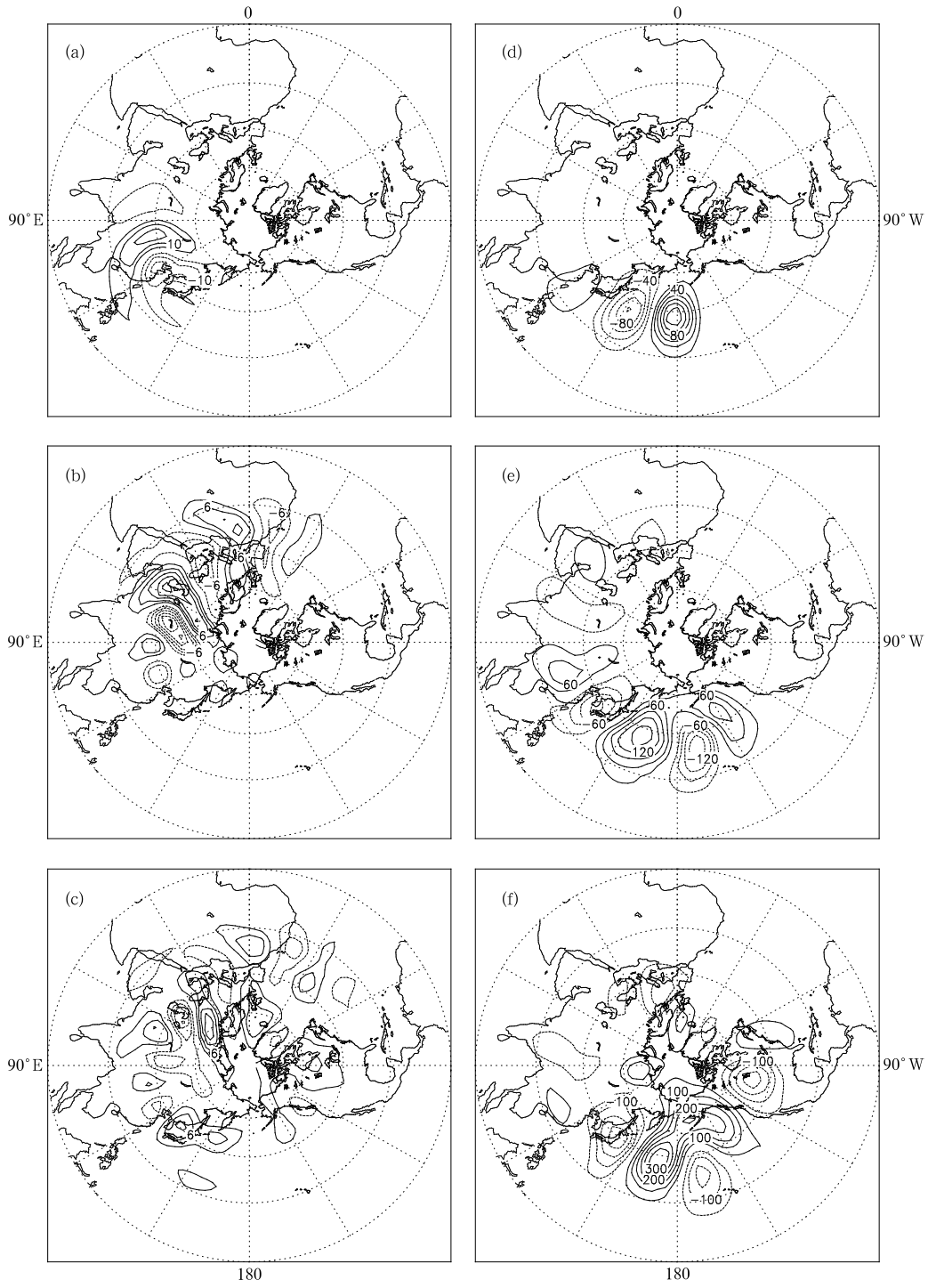

Fig. 3. As in Fig. 2, but for CNOPs.

vertical layers, we obtain

$$\frac{\partial \mathrm{TE}}{\partial t} = \left\langle \sum_{i=1}^{3} u_i' v_i' \left(\frac{\partial^2 \overline{\psi_i}}{\partial y^2} - \frac{\partial^2 \overline{\psi_i}}{\partial x^2}\right) \right\rangle + \left\langle \sum_{i=1}^{3} (u_i'^2 - v_i'^2) \frac{\partial^2 \overline{\psi_i}}{\partial x \partial y} \right\rangle - R_1^{-2} \langle (\psi_1' - \psi_2') \cdot \boldsymbol{V}_1' \nabla (\overline{\psi_1} - \overline{\psi_2}) \rangle - R_2^{-2} \left\langle (\psi_2' - \psi_3') \boldsymbol{V}_2' \cdot \nabla (\overline{\psi_2} - \overline{\psi_3}) \right\rangle + \left\langle \sum_{i=1}^{3} D_i' \psi_i' \right\rangle, \tag{2}$$

where

$$\mathrm{TE} = \frac{1}{2}\langle\sum_{i=1}^{3}\nabla^2\psi_i'\rangle + \frac{1}{2}R_1^{-2}\langle(\psi_1' - \psi_2')^2\rangle + \frac{1}{2}R_2^{-2}\langle(\psi_2' - \psi_3')^2\rangle.$$

TE is the total energy of the perturbations, including the kinetic and available potential energy. It is shown that the perturbation energy can grow through barotropic (the first two terms on the right hand side of Eq. (3)) and baroclinic (the third and fourth terms on the right hand side of Eq. (3)) extraction from the basic flow. The CNOP and SV present a northeast-southwest (northwest-southeast) trend in the north (south) flank of the jet in Figs. 2 and 3, which is favorable for the energy growth. For longer optimization time, more meridional extension of CNOP at the entrance of the jet may contribute to a larger energy growth rate than SV.

Figure 4 shows the total energy production of SV and CNOP for the optimization time of 2, 5, and 8 days, respectively. It is seen that for the optimal perturbations, the barotropic extraction is larger than baroclinic extraction from the basic flow. To be more precise, for day 2 shown in Fig. 4a, the kinetic (available potential) energy of SV is similar to that of CNOP during the evolution; while for the optimization time of 5 days in Fig. 4b, SV and CNOP have little difference in the kinetic (available potential) energy before day 3, but after that, both the kinetic and available potential energies of CNOP become larger than those of SV. Similarly, for the optimization time of 8 days in Fig. 4c, the kinetic energy of SV before day 5 is also almost the same as that of CNOP, and so is the available potential energy; however, after that, both the kinetic and available potential energies of CNOP become larger, and the total energy of CNOP is about two times of that of SV at the final time.

In addition, to examine the spatial distribution of energy evolution of the optimal perturbations, the energy spectra of the initial and final distributions of SVs and CNOPs are plotted in Fig. 5 as a function of the total wavenumber. Note that values at initial time are multiplied by 10 for optimization time of 2 days and 100 for optimization time of 5 and 8 days

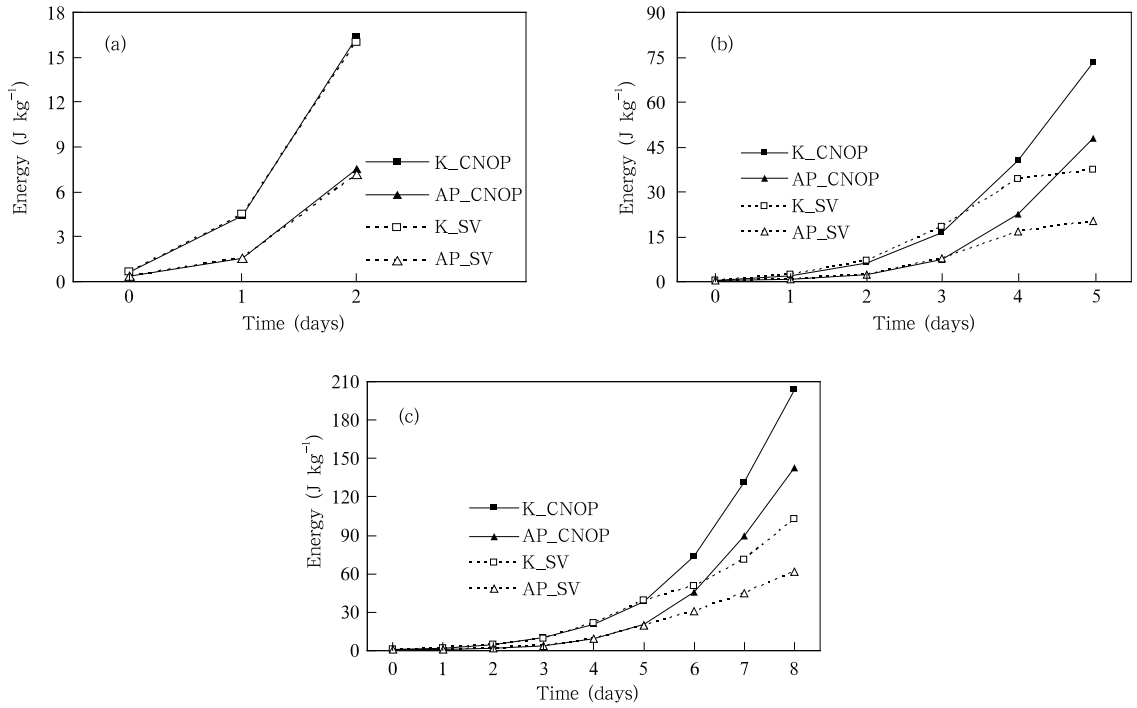

Fig. 4. The total energy (J kg^{-1}) of SV and CNOP with time for the optimization time of (a) 2, (b) 5, and (c) 8 days. K–SV (K–CNOP) represents the kinetic energy of the first SV (CNOP) and AP–SV (AP–CNOP) represents the available potential energy of the first SV (CNOP).

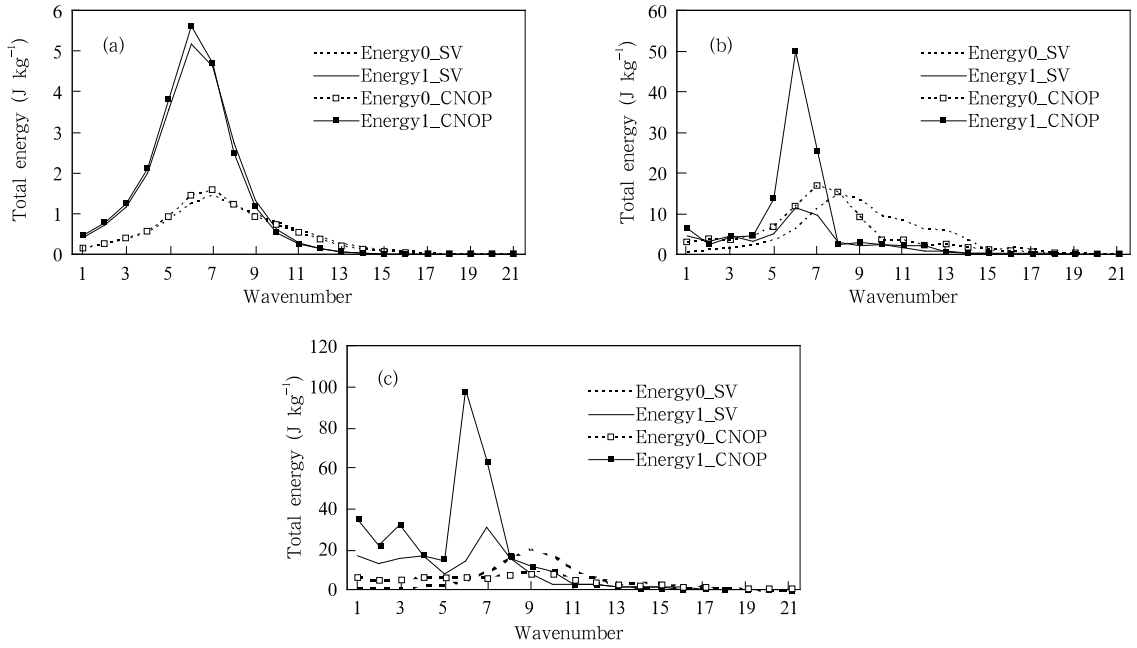

Fig. 5. The energy spectra (J kg^{-1}) of the initial and final distributions of SVs and CNOPs as a function of the total wavenumber for the optimization time of (a) 2, (b) 5, and (c) 8 days. Values at initial time are multiplied by 10 for optimization time of 2 days and 100 for optimization time of 5 and 8 days in order to plot them on the same scale as the final values. Energy0_SV (Energy0_CNOP) represents energy of the first SV (CNOP) at initial time and Energy1_SV (Energy1_CNOP) represents energy of the first SV (CNOP) at final time.

in order to plot them on the same scale as the final values. It is found that for the optimization time of 2 days in Fig. 5a, CNOP resembles SV. That is, the total energy peak falls on wavenumber 7 at initial time and wavenumber 6 at final time. When the optimization time extends into 5 days in Fig. 5b, the total energy peak for SV shifts to wavenumber 8 at initial time and others remain. For the optimization time of 8 days in Fig. 5c, the total energy peaks for both SV and CNOP fall on wavenumber 9 at initial time, and for SV (CNOP) on wavenumber 7 (6) at final time. However, the peak value for CNOP is higher than that for SV at final time for the same optimization time, which means that nonlinearity makes the energy more concentrated on one particular wavenumber. One common characteristic is that the energy peaks for both SV and CNOP concentrate on synoptic-scale waves and the scale amplification can be clearly seen from this figure. This is one possible reason why SVs and CNOPs are closely related to the transition of weather regimes (Molteni and Palmer, 1993; Mu and Jiang, 2008a).

5. The instability of the Eurasian atmospheric circulation

In this section, the effect of optimal perturbations on the Eurasian atmospheric circulation is investigated. Figure 6 shows the basic states of the streamfunction field perturbed by SVs and CNOPs at the optimization time of 2, 5, and 8 days. We find that great changes mainly occur with three weather systems over the Eurasian continent, including the blocking over the Asian continent, the East Asian major trough, and the northwestern Pacific subtropical high. For day 2 in Figs. 6a and 6d, the meridional flow over the Asian continent strengthens, the East Asian major trough deepens, and the northwestern Pacific subtropical high extends westward. For day 5 in Figs. 6b and 6e, the meridional flow over the Asian continent further strengthens, the East Asian major trough strongly deepens, and the northwestern Pacific

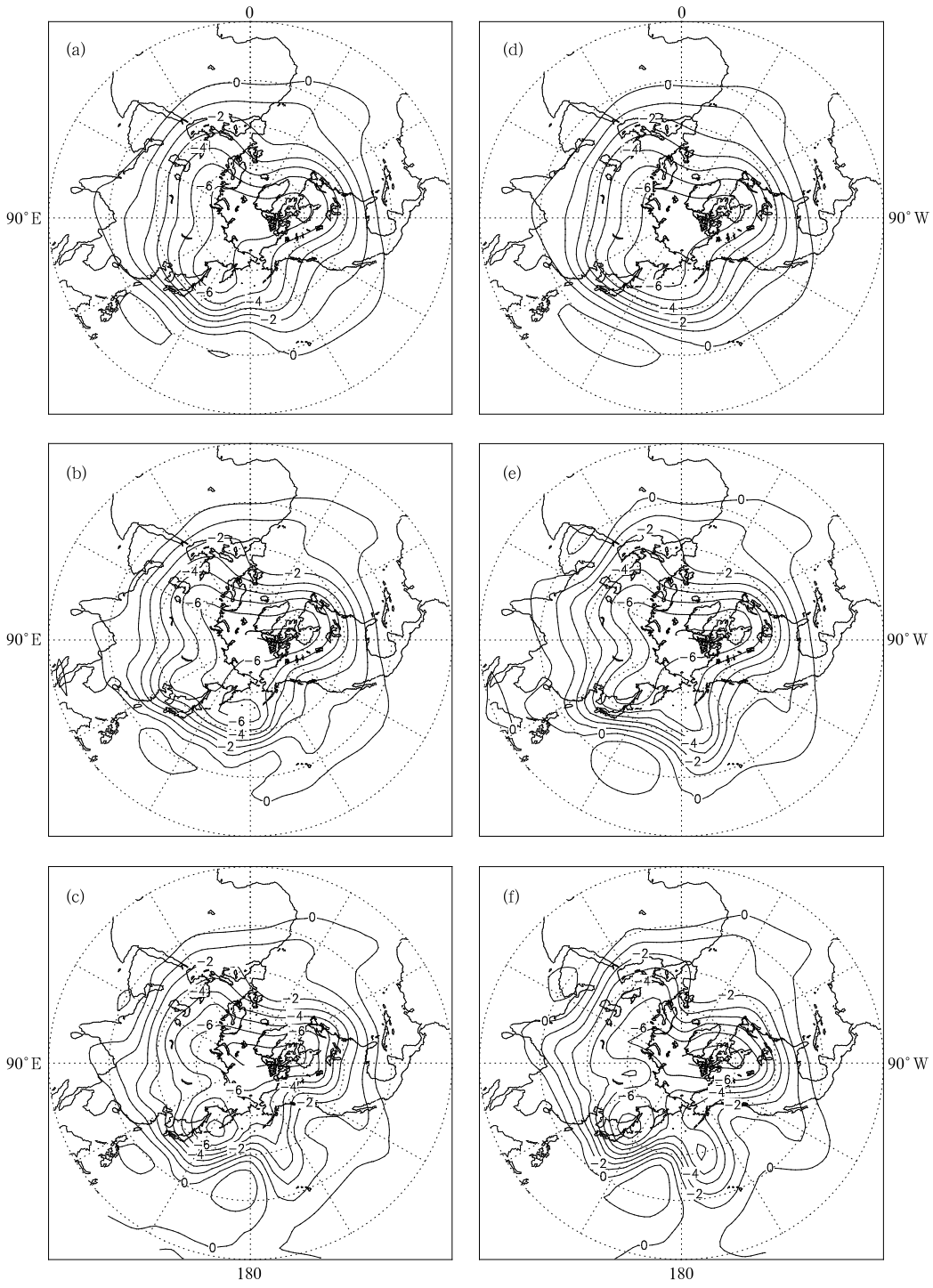

Fig. 6. The basic states of the streamfunction field ($\times 10^7 \mathrm{m}^{-2}\ \mathrm{s}^{-1}$) perturbed by the first SV at the optimization time of (a) 2 (b) 5, and (c) 8 days, and by CNOP at the corresponding optimization times (d–f).

subtropical high extends northward. Comparatively, the system perturbed by CNOP is stronger than that by SV. When the optimization time extends into 8 days (Figs. 6c and 6f), the East Asian major trough breaks into a low vortex, the northwestern Pacific subtropical high extends more northward, and the ridge

in the basic state perturbed by CNOP over the Asian continent evolves into a closed high pressure system over Lake Baikal. In the basic state perturbed by SV there appears only a ridge. In conclusion, the weather changes such as the blocking onset, the development of the major trough, and the movement of the northwestern Pacific subtropical high are closely related to the optimal perturbations. Comparatively, the CNOP method is a better tool for evaluation of the instability of the atmospheric circulation in the nonlinear regime.

6. Conclusions

In this paper, the finite-time instability revealed by use of SVs and CNOPs for a climatological flow is explored based on a three-level T21 QG model and its adjoint version. The results show that the most unstable region of the global atmospheric circulation lies in the midlatitude Eurasian continent. More specially, SV and CNOP at the optimization time of 2 days both present a property of localization: they are mainly located in the midlatitude Asian continent and its east coast. With extension of the optimization time, SVs are more upstream and less localized in the zonal direction, and CNOPs essentially differ from SVs with broader zonal and meridional extensions, presenting a northeast-southwest (northwest-southeast) trend in the north (south) flank of the entrance of the jet. Analysis of the energy growth reveals that the perturbation growth of SVs mainly comes from the kinetic energy, and the barotropic extraction from the basic flow plays a more important role. Comparatively, CNOPs obtain more energy growth in either the kinetic or available potential energy. It is shown that the instability of the atmospheric circulation is closely related to the jet in the westerly belt.

The spectrum analysis reveals that the wavenumber of total energy peaks for SV and CNOP increases with the increase of the optimization time. However, the energy peaks for SV and CNOP both concentrate on synoptic-scale waves, with increased spatial scales at final time. This may explain why SVs and CNOPs are closely related to the transition of weather regimes. SVs and CNOPs are successfully used as the initial ensemble perturbations for extreme weather forecasting in ECMWF and in preliminary ideal experiments as well (Mu and Jiang, 2008b).

The effects of optimal perturbations on the Eurasian atmospheric circulation are also studied. The results show that the instability of the Northern Hemispheric climatological circulation is concentrated over the Eurasian continent, including the appearance of strong meridional flow (even blocking high) over Lake Baikal, the deepening of the East Asian major trough, and the northward extension of the northwestern Pacific subtropical high. That is to say, the above three systems are closely related to the upstream midlatitude wave train structures. To obtain their stability, we also need to examine the upstream synoptic-scale wave activities. Moreover, how they interact with each other is worth further exploring. In addition, the weather systems over the Eurasian continent in the perturbed fields by CNOPs are stronger than those by SVs at the optimization time, indicating that the CNOP method is a better tool for evaluation of the instability of the Northern Hemispheric circulation in the nonlinear regime. The nonlinearity plays an important role in the weather regime transitions. Linear assumption underestimates the possibility of extreme weather events.

REFERENCES

Birgin, E. G., J. M. Martinez, and M. Raydan, 2000: Nonmonotone spectral projected gradient methods for convex sets. *SIAM Journal on Optimization*, **10**(4), 1196–1211.

Buizza, R., 1994: Sensitivity of optimal unstable structures. *Quart. J. Roy. Meteor. Soc.*, **120**, 429–451.

——, J. J. Tribbia, F. Molteni, and T. N. Palmer, 1993: Computation of optimal unstable structures for a numerical weather prediction model. *Tellus*, **45A**, 388–407.

Frederiksen, J. S., 2000: Singular vector, finite-time normal modes, and error growth during blocking. *J. Atmos. Sci.*, **57**, 312–333.

Jiang, Z. N., M. Mu, and D. H. Wang, 2008: Conditional nonlinear optimal perturbation of a T21L3 quasi-geostrophic model. *Quart. J. Roy. Meteor. Soc.*, **134**(633), 1027–1038.

Kim, H. M., M. C. Morgan, and R. E. Morss, 2004: Evolution of analysis error and adjoint-based sensi-

tivities: implications for adaptive observations. *J. Atmos. Sci.*, **61**(7), 795–812.

Li, Z. J., A. Barcilon, and I. M. Navon, 1999: Study of block onset using sensitivity perturbations in climatological flows. *Mon. Wea. Rev.*, **127**, 879–900.

Lorenz, E. N., 1963: Deterministic nonperiodic flow. *J. Atmos. Sci.*, **20**, 130–141.

——, 1965: A study of the predictability of a 28-variable model. *Tellus*, **17**, 321–333.

Marshall, J., and F. Molteni, 1993: Toward a dynamical understanding of planetary-scale flow regimes. *J. Atmos. Sci.*, **50**, 1792–1818.

Molteni, F., and T. N. Palmer, 1993: Predictability and finite-time instability of the northern winter circulation. *Quart. J. Roy. Meteor. Soc.*, **119**, 269–298.

Mu, M., W. S. Duan, and B. Wang, 2003: Conditional nonlinear optimal perturbation and its applications. *Nonlinear Processes in Geophysics*, **10**, 493–501.

—— and Z. Y. Zhang, 2006: Conditional nonlinear optimal perturbations of a two-dimensional quasigeostrophic model. *J. Atmos. Sci.*, **63**, 1587–1604.

—— and Z. N. Jiang, 2008a: A method to find perturbations that trigger blocking onset: conditional nonlinear optimal perturbations. *J. Atmos. Sci.*, **65**, 3935–3946.

—— and Z. N. Jiang, 2008b: A new approach to the generation of initial perturbations for ensemble prediction: conditional nonlinear optimal perturbations. *Chinese Science Bulletin*, **53**(13), 2062–2068.

Oortwijn, J., and J. Barkmeijer, 1995: Perturbations that optimally trigger weather regime. *J. Atmos. Sci.*, **52**(22), 3932–3944.

Riviere, O., G. Lapeyre, and O. Talagrand, 2008: Nonlinear generation of singular vectors: Behavior in a baroclinic unstable flow. *J. Atmos. Sci.*, **65**, 1896–1911.